Gain from cross talk among optical transitions

Sunish Menon[1] and G. S. Agarwal[1,2]

[1]*Physical Research Laboratory, Navrangpura, Ahmedabad 380 009, India*
[2]*Max-Plank-Institut für Quantenoptik, 85748 Garching, Germany*
(Received 27 July 1998)

We analyze the probe absorption spectra of a strongly driven Λ system with arbitrary spacing between the two lower levels. Under the condition that the spacing between the two lower levels is of the order of a strong-pump-field Rabi frequency, important interference effects are observed due to same-field coupling with both the transitions. We report the possibility of a significant gain from the *cross talk* among optical transitions, and a strong dependence of gain and absorption on the relative polarizations of the pump and probe beams. We present an analysis based on dressed states to explain our numerical results. [S1050-2947(99)01801-6]

PACS number(s): 42.50.Gy, 42.50.Hz

I. INTRODUCTION

The very early work of Mollow [1] on a coherently driven two-level atom demonstrated the possibility of gain without inversion in bare states. Mollow's work led to a variety of experimental [2] and theoretical [3] activity on gain in driven systems. Various features of gain in driven two-level systems are now understood [4–6] both in terms of inversion in a dressed basis or in terms of coherence in the new basis. In the last decade the work on gain in driven systems became especially important with the work of Harris [7] and Kocharovskaya and Khanin [8] on lasing without population inversion (LWI). Harris in particular emphasized how the interference effects can make the absorption and emission profiles asymmetric, leading to the possibility of gain without inversion. Many different models for LWI have been proposed [9–13], and several experiments [14–16] were also performed to test these ideas. Gain can be understood to be arising either from inversion between dressed states or from coherence between such states. For the model of Ref. [9], coherence plays a very important role [17].

In connection with LWI models, one usually considers the interaction of a strong coherent drive and a weak probe with different transitions of a system, i.e., the pump and probe act on different transitions. There are, however, situations when one has to relax the above assumption. Consider for example the hyperfine levels of potassium, the excited level $4P_{1/2}(F=1)$ and the two ground levels $4S_{1/2}(F=2)$ and $4S_{1/2}(F=1)$ (Λ system), where the ground-level splitting is of the order of 462 MHz for ^{39}K, and 254 MHz for ^{41}K. In such case a single field can couple with more than one transition, and unlike driven two-level where doublets of dressed levels appear around bare levels, now multiple dressed levels appear [18–20], giving rise to many additional features. Along with this, for a probe field scanning such a system, interference effects become inevitable due to the strong coherence between the two closely spaced ground levels. This coherence is created due to the cross talk among optical transitions.

It may be noted that such common coupling of levels in a Λ system was studied in the context of optical bistability [21] and two-photon gain [22]. Xia *et al.* demonstrated the possibility of electromagnetically induced transparency [23]

in the presence of common coupling among hyperfine levels of ^{207}Pb. In this paper, we present the effects of such common coupling on probe response in a driven system with closely spaced ground levels, particularly when ground levels have *a separation of the order of driving field Rabi frequency.*

The organization of this paper is as follows: In Sec. II we study the absorption and gain spectra of a strongly driven three-level atom, and show the possibility of significant gain in such a medium. We include the effect of cross talk among optical transitions. In Sec. III we analyze the spectra by identifying strong interference effects, which gives rise to more pronounced gain when spacing between the two ground levels is of the order of one-half the pump Rabi frequency. In Sec. IV we present the dressed-state analysis to understand the numerical results. We show the existence of gain features due to inversion in dressed states, and transparency at certain probe frequencies due to weak coupling among dressed states.

II. MODEL SYSTEM

We select a Λ system with one excited state $|1\rangle$, and two ground levels $|2\rangle$ and $|3\rangle$ (see Fig. 1) with arbitrary spacing Ω between them. Such a configuration of levels with two fields has been well studied by assuming that a given field is driving *only one transition.* This can be achieved either by selecting levels with large spacing Ω or by suitable arrange-
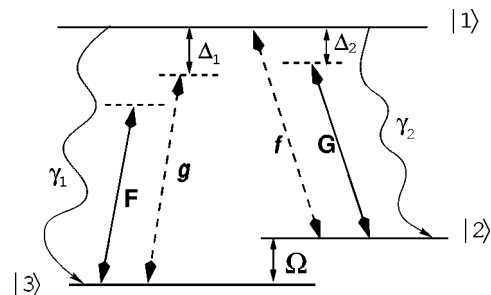

FIG. 1. Schematic diagram of a three-level Λ system with arbitrary spacing Ω between the two ground levels. The pump (coupling strengths F and G) and probe fields (coupling strengths g and f) act on both the transitions.

ment of field polarization. However, in this particular case we allow the same field to act on both the transitions, i.e., the pump field, $\vec{\mathcal{E}}_2 = \vec{E}_2 e^{-i\omega_2 t} + \text{c.c.}$, which is driving the $|1\rangle \leftrightarrow |2\rangle$ transition (Rabi frequency, $2G = 2\vec{E}_2 \cdot \vec{d}_{12}/\hbar$), can also couple with the $|1\rangle \leftrightarrow |3\rangle$ transition (Rabi frequency, $2F = 2\vec{E}_2 \cdot \vec{d}_{13}/\hbar$). Similarly, the weak probe field, $\vec{\mathcal{E}}_1 = \vec{E}_1 e^{-i\omega_1 t} + \text{c.c.}$ applied on the $|1\rangle \leftrightarrow |3\rangle$ transition (Rabi frequency, $2g = 2\vec{E}_1 \cdot \vec{d}_{13}/\hbar$) can also drive the $|1\rangle \leftrightarrow |2\rangle$ transition (Rabi frequency, $2f = 2\vec{E}_1 \cdot \vec{d}_{12}/\hbar$). Here $\vec{d}_{ij}$ is the electric transition dipole moment between states $|i\rangle$ and $|j\rangle$.

The Hamiltonian, $\mathcal{H}$ for this system in the dipole approximation is

$$\mathcal{H} = \hbar W_{13} A_{11} + \hbar \Omega A_{22} - (\vec{d}_{12} A_{12} + \vec{d}_{13} A_{13} + \text{H.c.}) \cdot (\vec{E}_2 e^{-i\omega_2 t}$$
$$+ \vec{E}_1 e^{-i\omega_1 t} + \text{c.c.}), \tag{1}$$

where the zero of energy is defined at $|3\rangle$, and $\hbar W_{13}$ is the energy difference between states $|1\rangle$ and $|3\rangle$. Here the fields are treated classically, and $A_{ij} = |i\rangle\langle j|$ represents the atomic population operators for $i = j$ and transition operators for $i \neq j$. The state $|\psi\rangle$ of this system is the solution of the Schrödinger equation

$$i\hbar \frac{\partial |\psi\rangle}{\partial t} = \mathcal{H}|\psi\rangle. \tag{2}$$

Under a unitary transformation, $|\phi\rangle = e^{i\omega_2 A_{11} t}|\psi\rangle$, the Schrödinger equation (2) for $|\phi\rangle$ will have the effective Hamiltonian $\mathcal{H}' = -\hbar\omega_2 A_{11} + e^{i\omega_2 A_{11} t}\mathcal{H}e^{-i\omega_2 A_{11} t}$, given by

$$\mathcal{H}'/\hbar = (\Delta_2 + \Omega)A_{11} + \Omega A_{22} - (G + f e^{-i\omega_{12}t})A_{12}$$
$$- (F + g e^{-i\omega_{12}t})A_{13} + \text{H.c.}, \tag{3}$$

where $\omega_{12} = \omega_1 - \omega_2$ is the probe-pump detuning. Note that the the pump detuning for the transition $|1\rangle \leftrightarrow |2\rangle$, $\Delta_2 = W_{13} - \Omega - \omega_2$, along with the probe detuning for the transition $|1\rangle \leftrightarrow |3\rangle$, $\Delta_1 = W_{13} - \omega_1$, satisfy the relation $\omega_{12} = \Delta_2 - \Delta_1 + \Omega$. We take $G, F \ll \omega_2, \omega_1$, and hence neglect the rapidly oscillating terms like $\omega_1 + \omega_2, 2\omega_2, 2\omega_1$ in (3) by invoking the rotating-wave approximation (RWA).

We include the natural decay terms in our analysis, and hence use the density-matrix formalism. Let $2\gamma_2$ and $2\gamma_1$ denote the spontaneous emission rates from state $|1\rangle$ to the states $|2\rangle$ and $|3\rangle$ respectively. The density-matrix equations will be

$$\dot{\rho}_{11} = -2(\gamma_1 + \gamma_2)\rho_{11} + i(F + g e^{-i\omega_{12}t})\rho_{31}$$
$$+ i(G + f e^{-i\omega_{12}t})\rho_{21} - i(G^* + f^* e^{i\omega_{12}t})\rho_{12}$$
$$- i(F^* + g^* e^{i\omega_{12}t})\rho_{13},$$

$$\dot{\rho}_{22} = 2\gamma_2 \rho_{11} + i(G^* + f^* e^{i\omega_{12}t})\rho_{12} - i(G + f e^{-i\omega_{12}t})\rho_{21},$$

$$\dot{\rho}_{33} = 2\gamma_1 \rho_{11} + i(F^* + g^* e^{i\omega_{12}t})\rho_{13} - i(F + g e^{-i\omega_{12}t})\rho_{31},$$

$$\dot{\rho}_{12} = -(\gamma_1 + \gamma_2 + i\Delta_2)\rho_{12} + i(F + g e^{-i\omega_{12}t})\rho_{32}$$
$$- i(G + f e^{-i\omega_{12}t})(\rho_{11} - \rho_{22}), \tag{4}$$

$$\dot{\rho}_{13} = -(\gamma_1 + \gamma_2 + i(\Delta_2 + \Omega))\rho_{13} + i(G + f e^{-i\omega_{12}t})\rho_{23}$$
$$- i(F + g e^{-i\omega_{12}t})(\rho_{11} - \rho_{33}),$$

$$\dot{\rho}_{23} = -i\Omega\rho_{23} + i(G^* + f^* e^{i\omega_{12}t})\rho_{13} - i(F + g e^{-i\omega_{12}t})\rho_{21}.$$

Note that the density-matrix elements in the original frame are given by $\rho_{12} e^{-i\omega_2 t}$, $\rho_{13} e^{-i\omega_2 t}$, ρ_{23}, ρ_{11}, ρ_{22}, and ρ_{33}.

The well-known result for such a model (without the probe field) is the Raman (Stokes and anti-Stokes) and Rayleigh lines observed in the fluorescence spectrum when $F, G < \gamma_1, \gamma_2 \ll |\Omega|$. Cohen-Tannoudji and Reynaud [20] studied a similar situation—the changes in the Raman and Rayleigh lines at pump intensities much above the saturation intensity. They specifically studied the two extreme cases $|\Omega| \gg F, G \gg \gamma_1, \gamma_2$ and $F, G \gg \gamma_1, \gamma_2 \gg |\Omega|$ and noted the mixing of Raman and Rayleigh lines in the latter case. They also discussed the probe absorption characteristics in the above limits. Our interest lies in the case when $|\Omega| \approx F, G \gg \gamma_1, \gamma_2$. For hyperfine splittings, like the one in potassium, one can easily have field strengths such that $F, G \approx |\Omega|$. Other possibilities will include Zeeman levels in the presence of a magnetic field, and linearly polarized electromagnetic fields. The radiative decay terms in Eq. (4) ignores the effects of spontaneously generated coherence [24] as in most atomic systems the two transition dipole moments $\vec{d}_{12}$ and $\vec{d}_{13}$ will be orthogonal. Expanding the solutions of Eqs. (4) in terms of the harmonics of ω_{12},

$$\rho_{ij} = \sum_m \rho_{ij}^{(m)} e^{-im\omega_{12}t}, \tag{5}$$

the set of equations for $\rho_{ij}^{(m)}$ can be solved for the steady state. Since the probe field is assumed to be weak enough $(F, G \gg \gamma_1, \gamma_2 \gg f, g)$, a perturbative solution will result only in the harmonics corresponding to $m = \pm 1$ in Eq. (5). The probe field absorption $\mathcal{A}$ per unit volume due to the average induced polarization $\vec{\mathcal{P}}$ is

$$\mathcal{A} = \overline{\vec{\mathcal{E}}_1 \cdot \frac{\partial \vec{\mathcal{P}}}{\partial t}}, \tag{6}$$

where the bar denotes the time average. The average polarization for $\mathcal{N}$ atoms per unit volume is

$$\vec{\mathcal{P}} = \mathcal{N}\{\vec{d}_{21}\rho_{12}e^{-i\omega_2 t} + \vec{d}_{31}\rho_{13}e^{-i\omega_2 t} + \text{c.c.}\}. \tag{7}$$

Here ρ_{ij}'s are the steady-state solutions of Eqs. (4). The probe absorption, using Eqs. (5), (6), and (7), is

$$\mathcal{A} = \mathcal{N}\hbar\{i\omega_1[g\rho_{31}^{(-1)} + f\rho_{21}^{(-1)} - g^*\rho_{13}^{(+1)} - f^*\rho_{12}^{(+1)}]$$
$$+ i\omega_2[(g\rho_{31}^{(0)} + f\rho_{21}^{(0)})\overline{e^{-i\omega_{12}t}} - (g^*\rho_{13}^{(0)} - f^*\rho_{12}^{(0)})\overline{e^{i\omega_{12}t}}]\}, \tag{8}$$

The energy absorption per unit volume is

$$\mathcal{A} = i\mathcal{N}\hbar\omega_1[g\rho_{13}^{*(+1)} + f\rho_{12}^{*(+1)} - g^*\rho_{13}^{(+1)} - f^*\rho_{12}^{(+1)}], \tag{9}$$

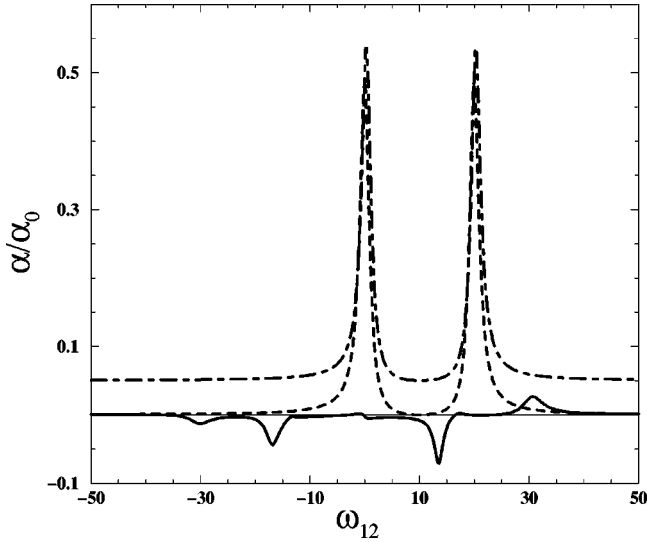FIG. 2. Probe absorption coefficient α in dimensionless units as a function of probe-pump detuning ω_{12} for a driven Λ system with near-degenerate ground levels (solid curve). The parameters are $G = F = 10$, $g = f = 0.1$, $\Delta_2 = 0$, and $\Omega = 10$. For comparison we also plot (dashed curve) the usual Autler-Townes components observed when $F = f = 0$. For large separation between $|2\rangle$ and $|3\rangle$, $\Omega = 500$, the gain disappears (dot-dashed) and the standard Autler-Townes splitting emerges. For this case we have shifted the X axis by -490 units, and the Y axis by 0.05 units for clarity and comparison. These structures otherwise appear at $\omega_{12} = \Omega \pm G$. All frequencies are in units of $\gamma_1 = \gamma_2 = \gamma$.

where we use the fact that $\rho_{ij} = \rho_{ji}^*$. The probe absorption coefficient α per unit length (the ratio of $\mathcal{A}$ and the input probe intensity $c|E_1|^2/2\pi$) is

$$\alpha = \frac{\alpha_0}{g^2}[g\gamma_1 \mathrm{Im}(\rho_{13}^{(+1)}) + f\gamma_1 \mathrm{Im}(\rho_{12}^{(+1)})], \qquad (10)$$

where we treat the probe Rabi frequencies as real, $\alpha_0 = 4\pi\mathcal{N}\omega_1|d_{13}|^2/c\gamma_1\hbar$, and c is the velocity of light in vacuum. Note that the absorption now involves both $\mathrm{Im}(\rho_{12}^{(+1)})$ and $\mathrm{Im}(\rho_{13}^{(+1)})$ because the probe is acting on both the transitions.

We take the polarization of both pump and probe fields along $(\hat{\boldsymbol{\epsilon}}_2 + \hat{\boldsymbol{\epsilon}}_3)/\sqrt{2}$ (except in Fig. 6) where $\hat{\boldsymbol{\epsilon}}_2$ and $\hat{\boldsymbol{\epsilon}}_3$ are unit vectors along $\vec{d}_{12}$ and $\vec{d}_{13}$ ($\vec{d}_{12} \perp \vec{d}_{13}$), respectively. For simplicity we take $\gamma_1 = \gamma_2 = \gamma$ and scale the Rabi frequencies, detunings, and Ω by γ. Also, for our numerical work we take $G = F$ and $g = f$. In Fig. 2, the probe absorption coefficient is shown in units of α_0 as a function of probe-pump detuning ω_{12} for $\Omega = G$. The negative absorption in the profile corresponds to stimulated emission. *The solid curve in Fig. 2 shows the remarkable result that cross talk between different optical transitions gives rise to gain, provided the energy separation between the two ground levels is of the order of one-half the pump Rabi frequency.* When cross talk is not taken into account, as shown in the figure, one observes the usual Autler-Townes [25] components.

The complex linear susceptibility χ ($\vec{\mathcal{P}} = \chi\vec{\mathcal{E}}_1$) is given by
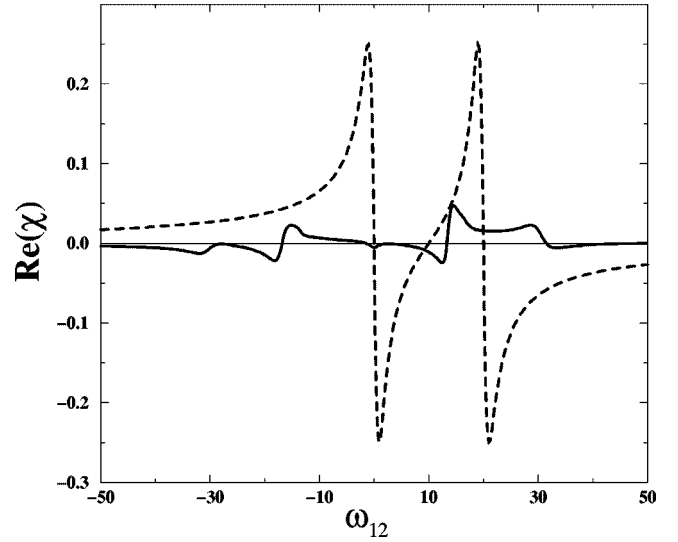

FIG. 3. Real χ in units of $\mathcal{N}|\vec{d}_{13}|^2/\gamma_1\hbar$. The common parameters are $G = \Omega = 10$, $g = 0.1$, and $\Delta_2 = 0$. The solid curve has $F = 10$, and $f = 0.1$, and the dashed curve is for $F = f = 0$.

$$\chi = \frac{\mathcal{N}|\vec{d}_{13}|^2}{\gamma_1\hbar g^2}[g\gamma_1\rho_{13}^{(+1)} + f\gamma_1\rho_{12}^{(+1)}]. \qquad (11)$$

The dispersion properties of the medium corresponding to the real part of χ are plotted in Fig. 3, both in the presence and absence of cross talk. Clearly, the cross talk also significantly changes the dispersion characteristics. The imaginary part of χ corresponds to absorption, as can be seen from Eq. (10).

Three gain peaks along with an absorption peak and a central dispersive profile are the clear features of the solid curve in Fig. 2. The dispersive gain around $\omega_1 \approx \omega_2$ is a kind of stimulated Rayleigh gain, also seen in a driven two-level. The origin of such dispersive features are known [4,5], and lasing based on similar dispersive gain mechanism has been discussed in the past [26]. The features at the two extremes will show gain or absorption depending on the pump detuning. They appear as dispersive profiles when pump field is tuned to the center of $|2\rangle$ and $|3\rangle$, as shown in Fig. 4. The spectra is symmetric about $\omega_{12} = 0$ for this detuning. On the other hand the two intermediate gain regions depend significantly on the pump Rabi frequency. These gains are maximum for $|\Omega| \approx G = F$, and disappear for both $|\Omega| \gg G,F$ and $|\Omega| \ll G,F$. The gain is observed for both $\omega_{12} > 0$ and $\omega_{12} < 0$ for a given pump detuning, and this supplements to the recently observed gain by Brown *et al.* [27].

It should be noted that these gains are not because of any inversion in the bare states. The steady-state population in the three bare states and the ground-state coherence in the absence of probe field is

$$\rho_{11}^{(0)} = \frac{2G^2\Omega^2}{8G^4 + 8\Omega^2 + 2G^2\Omega^2 + \Omega^4},$$

$$\rho_{22}^{(0)} = \frac{4G^4 + 4\Omega^2 + G^2\Omega^2}{8G^4 + 8\Omega^2 + 2G^2\Omega^2 + \Omega^4},$$
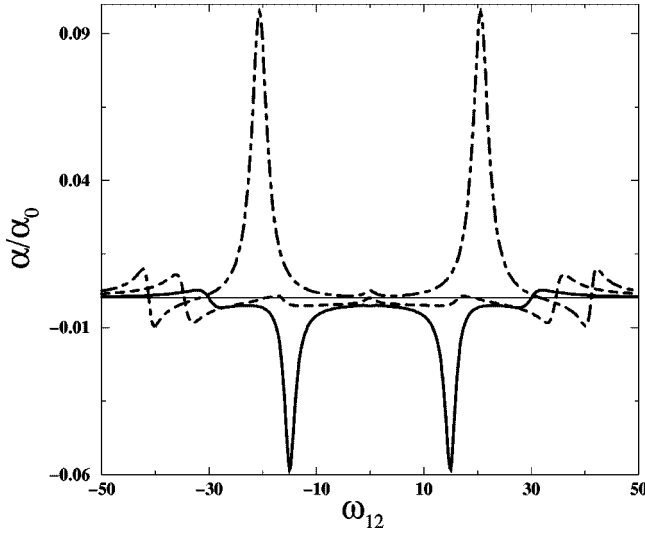
$$(12)$$

FIG. 4. Probe absorption spectra for various values of Ω when the pump field is tuned to the center of states $|2\rangle$ and $|3\rangle$ ($\Delta_2 = -\Omega/2$). The solid curve is for $\Omega = G$, the dashed curve for $\Omega = 2G$, and the dot-dashed curve for $\Omega = 3G$. The parameters are $F = G = 10$ and $f = g = 0.1$. The two intermediate gains appear as dispersive profiles at $\Omega = 2G$ and for $\Omega > 2G$; these regions show absorption features. Note that the dispersive profiles at the two extremes do not show such crucial dependence on the pump field strength.

$$\rho_{33}^{(0)} = \frac{4G^4 + \Omega^4 + 4\Omega^2 - G^2\Omega^2}{8G^4 + 8\Omega^2 + 2G^2\Omega^2 + \Omega^4},$$

$$\rho_{23}^{(0)} = \frac{G^2(\Omega^2 - 4G^2 + 4i\Omega)}{8G^4 + 8\Omega^2 + 2G^2\Omega^2 + \Omega^4},$$

where we take $F = G$, $\Delta_2 = 0$, and $\gamma = 1$ as in Fig. 2. Comparing the numerators, it can be shown from the above expressions that (i) $\rho_{33}^{(0)} > \rho_{11}^{(0)}$ for all values Ω and (ii) $\rho_{22}^{(0)} > \rho_{11}^{(0)}$ for $\Omega < 2G$. Note that the coherence $|\text{Re}(\rho_{23}^{(0)})|$ is significant only for the range of $|\Omega| < 2G$, and is negligible for $\Omega \gg 2G$. We show in Sec. III that this coherence can give rise to gain.

III. NEW INTERFERENCE EFFECTS

We next analyze the spectra in Fig. 2, and will isolate the new features as due to interference effects arising from cross talk among optical transitions. To see this, we separate the different effects of the probe field on the two transitions $|1\rangle \leftrightarrow |2\rangle$ and $|1\rangle \leftrightarrow |3\rangle$ by writing $\rho_{ij}^{(+1)} = g\sigma_{ij} + f\sigma'_{ij}$ and $\rho_{ij}^{(-1)} = g\sigma_{ji}^* + f\sigma'_{ji}^*$. Here we again use $\rho_{ij} = \rho_{ji}^*$ to write the latter part, and treat f and g as real. The probe absorption coefficient α in this case will be

$$\alpha = \frac{\alpha_0 \gamma_1}{g^2} [g^2 \text{Im}(\sigma_{13}) + f^2 \text{Im}(\sigma'_{12})$$

$$+ fg\,\text{Im}(\sigma_{12}) + fg\,\text{Im}(\sigma'_{13})], \qquad (13)$$

where the first two terms correspond to *absorption* along $|1\rangle \leftrightarrow |3\rangle$ and $|1\rangle \leftrightarrow |2\rangle$ transitions. The last two terms corre-

spond to an *interference* among the probe field along the two transitions—a result of cross talk among the two transitions. As observed, this interference term plays a prominent role for small Ω, and disappears for large Ω. For our numerical results we separate out the contribution of the direct *absorption* term and the *interference* term in Eq. (13). In Fig. 5 we plot the net absorption coefficient along with the contribution of absorption and interference terms. Note that the gain peaks around $\omega_{12} = -16.8$ and 13.5 are *enhanced* by the interference. On the other hand, the strong absorptions around $\omega_{12} = -13.3$ and 16.6 are almost *nullified* by the interference, though the refractive index (see Fig. 3, especially in the
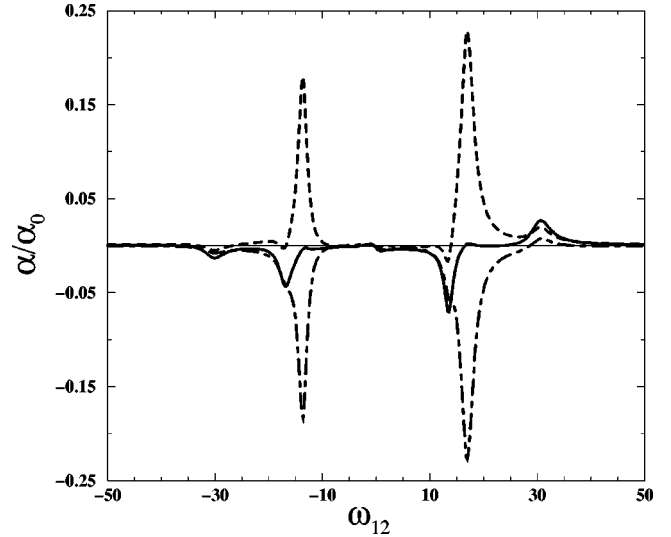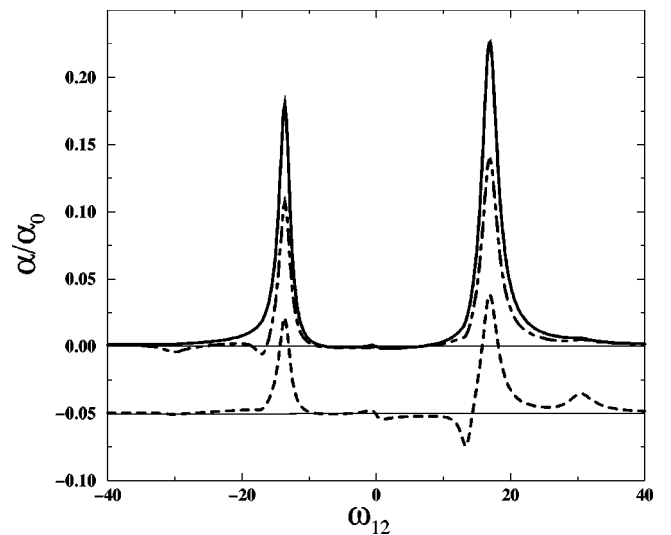

FIG. 5. Probe absorption spectra for $\Omega = G = F = 10$. The interference term (dot-dashed curve) and the absorption term (dashed curve), as in Eq. (13), are separated to see their individual contribution on the net result (solid curve). The remaining parameters are $\Delta_2 = 0$ and $f = g = 0.1$, and all parameters are in units of γ.

FIG. 6. Probe absorption for different orientation of probe field $\vec{E}_1$ with respect to the pump field $\vec{E}_2$. The solid curve is for $f = -g$, the dashed curve for $f = 0$ (shifted by -0.05 units along the Y axis for clarity), and the dot-dashed curve for $g = 0$. For all the cases $\vec{E}_2$ is along an axis at 45° to both $\vec{d}_{12}$ and $\vec{d}_{13}$. The remaining parameters are as in Fig. 5.
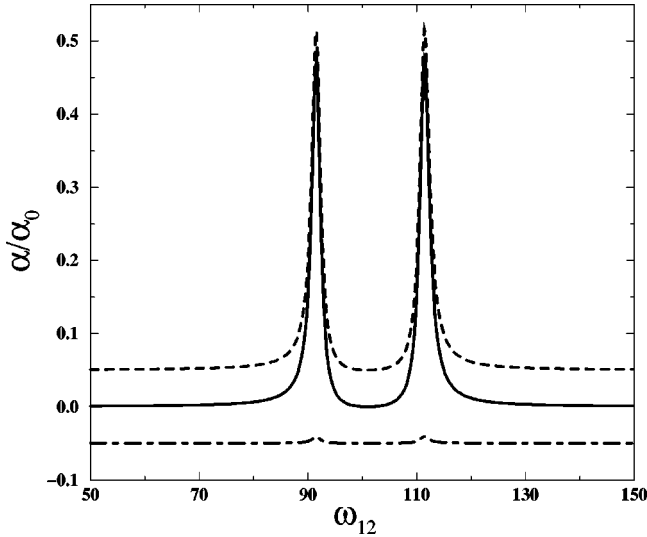
FIG. 7. Probe absorption spectra for $\Omega = 100$. The interference term (dot-dashed curve) is displaced by -0.05 units and the absorption term (dashed curve) by $+0.05$ units along the Y axis for clarity. The net result is the solid curve. The other parameters are as in Fig. 5. Note that the interference contribution is negligible, and one observes the usual Autler-Townes components at $\omega_{12} = \Omega \pm G$ for this set of parameters.

region $17 \lesssim \omega_{12} \lesssim 25$) is still large. The interference thus leads to dispersion enhancement in the region of very low absorption as has been realized earlier by Scully [28] for a somewhat different model. The interference term is also sensitive to the relative orientation of the probe and pump field polarizations. In Fig. 6 we show the probe absorption for various probe polarizations. When the pump and probe are perpendicular to each other ($f = -g$), the interference term will flip to give rise to strong absorption [29]. In Fig. 6 we also show the result when probe acts only on transition $|1\rangle \leftrightarrow |3\rangle$ ($f = 0$) or $|1\rangle \leftrightarrow |2\rangle$ ($g = 0$).

The origin of interference can be understood by explicitly writing down the equations of density matrix elements appearing in Eq. (13):

$$\dot{\sigma}'_{12} = -(\gamma_1 + \gamma_2 + i(\Delta_1 - \Omega))\sigma'_{12}$$
$$+ iF\sigma'_{32} - iG(\sigma'_{11} - \sigma'_{22}) - i(\rho_{11}^{(0)} - \rho_{22}^{(0)}),$$

$$\dot{\sigma}_{12} = -(\gamma_1 + \gamma_2 + i(\Delta_1 - \Omega))\sigma_{12}$$
$$+ iF\sigma_{32} - iG(\sigma_{11} - \sigma_{22}) + i\rho_{32}^{(0)}, \qquad (14)$$

$$\dot{\sigma}_{13} = -(\gamma_1 + \gamma_2 + i\Delta_1)\sigma_{13} + iG\sigma_{23}$$
$$- iF(\sigma_{11} - \sigma_{33}) - i(\rho_{11}^{(0)} - \rho_{33}^{(0)}),$$

$$\dot{\sigma}'_{13} = -(\gamma_1 + \gamma_2 + i\Delta_1)\sigma'_{13} + iG\sigma'_{23} - iF(\sigma'_{11} - \sigma'_{33}) + i\rho_{23}^{(0)}.$$

The behavior of the elements in the interference term (σ_{12}, σ'_{13}) is governed by the zeroth-order coherence between states $|2\rangle$ and $|3\rangle$, created by the pump field. On the other hand, the elements in the absorption term depends on the zeroth-order inversion terms.

In order to understand the contribution of the interference term in detail, we look at large and intermediate values of Ω as compared to the pump Rabi frequency. A large Ω and small Δ_2 effectively correspond to the case when the pump is tuned to one transition, and in this case one does not expect any coherence due to cross talk among transitions. Figure 7 shows the Autler-Townes components at $\Delta_1 = -\frac{1}{2}(\Delta_2 \mp \sqrt{\Delta_2^2 + 4G^2})$. At $\omega_{12} = \Omega$ ($\Delta_1 = \Delta_2$) the figure shows the transparency point due to coherent population trapping [30]. Note that the contribution from the interference term is negligible in this case.

For intermediate values of Ω, the pump at both the transitions has to be considered, and, depending on the probe detuning, one expects two sets of Autler-Townes components (Fig. 8). The transparency points will be seen at $\omega_{12} = \pm \Omega$ (at $\Delta_1 = \Delta_2$ and $\Delta_1 - \Omega = \Delta_2 + \Omega$) as shown in Fig. 9. The gain for the Autler-Townes components around $\omega_{12} = -\Omega$ is because of the resonant pump field G at $|1\rangle \leftrightarrow |2\rangle$ transition ($\Delta_2 = 0$ for Fig. 9). Also seen in Fig. 9 are Mollow [1] kind of features around $\omega_{12} = \pm 2G, 0$, due to the probe tuning to the same transition to which pump is tuned. In this case the third effectively nonparticipating level acts like a sink, resulting in very diminished features. These features can also be interpreted in terms of Raman and Rayleigh peaks due to pump intensities much above the saturation intensity [20].

For Ω close to G all the features discussed above are significant, and they are superimposed over one another. The coherence between states $|2\rangle$ and $|3\rangle$ also increases due to cross talk. Thus the interference term plays a dominant role as shown in Fig. 5, giving rise to stimulated emission. If Ω is reduced further, strong absorption and interference features are seen around $\omega_{12} \approx \sqrt{2}G$. At $\Omega = 0$ the interference term completely cancels the absorption, as shown in Fig. 10. This transparency is due to the phenomenon of coherent population trapping (CPT) [30].

IV. SEMICLASSICAL DRESSED STATES

We examine the impact of the coherence created by cross talk in a dressed basis. In particular, to understand the pres-
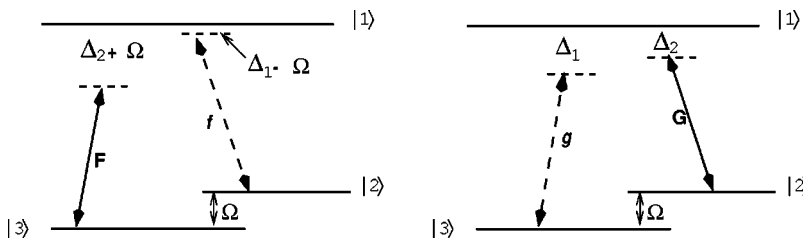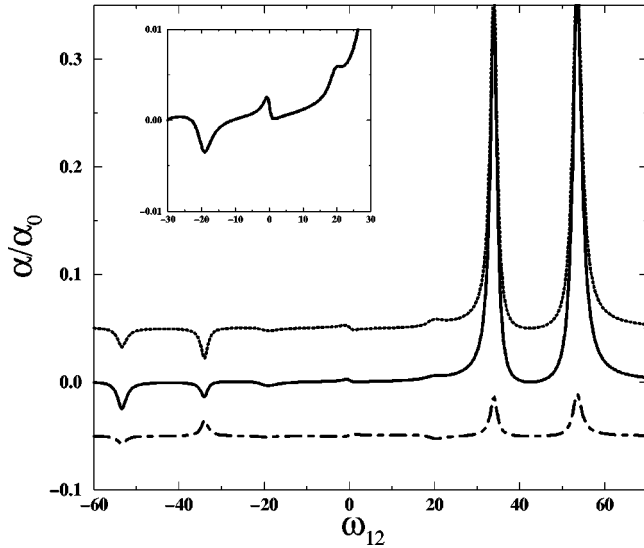

FIG. 8. The two effective 3 levels, depending on the probe detuning for intermediate values of $|\Omega|$. Two sets of Autler-Townes components will be seen depending on which transition the probe is tuned to.

FIG. 11. (a) The bare states in the rotating frame. (b) The corresponding semiclassical dressed states for $\Omega > 0$. The energy in units of $\hbar$ is given on the left side of the levels.

$$i\dot{C} = HC, \qquad (16)$$

where C and H are 3×1 and 3×3 matrices:

$$C = \begin{bmatrix} C_1(t) \\ C_2(t) \\ C_3(t) \end{bmatrix}, \quad H = \begin{bmatrix} \Omega & -G & -F \\ -G & \Omega & 0 \\ -F & 0 & 0 \end{bmatrix}. \qquad (17)$$

The dressed-state analysis involves the evaluation of stationary states for the atom plus pump field system. The matrix Hamiltonian in Eq. (17) can be diagonalized by taking $\det|H - I\lambda| = 0$. This will result in a cubic equation of the form $\lambda^3 + A\lambda^2 + B\lambda + C = 0$ where $A = -2\Omega, B = \Omega^2 - F^2 - G^2$, and $C = \Omega F^2$. The two extreme roots of the above cubic equation are

$$\lambda_\pm = -A/3 \pm \tfrac{2}{3}\sqrt{(A^2 - 3B)} \cos[\tfrac{1}{3}\cos^{-1}(\mp L)], \qquad (18)$$

where $L = (27C + 2A^3 - 9AB)/2(A^2 - 3B)^{3/2}$, and the third root is $\lambda_0 = -A - \lambda_+ - \lambda_-$. The dressed levels are schematically shown in Fig. 11. In Figs. 12(a) and 12(b), we plot the eigenvalues as a function of Ω for $\Delta_2 = 0$ and $-\Omega/2$. For small Ω, $\lambda_0 \to 0$. At $\Omega = 0$ the eigenvalues $\lambda_\pm$ are symmetrically situated about λ_0 for case (a), but for case (b) this symmetry is maintained for the entire range of Ω. For large Ω either λ_+ or λ_- goes to zero, and hence the corresponding eigenstate becomes the ground state $|3\rangle$. The two remaining excited eigenstates gives rise to the Autler-Townes components.

Physically the above eigenvalue analysis means a unitary transformation of the Hamiltonian $H \to SHS^\dagger$ where S is the unitary matrix given by

$$S = \begin{bmatrix} -G\lambda_+ N_+ & (\lambda_+(\lambda_+ - \Omega) - F^2)N_+ & FGN_+ \\ -G\lambda_0 N_0 & (\lambda_0(\lambda_0 - \Omega) - F^2)N_0 & FGN_0 \\ -G\lambda_- N_- & (\lambda_-(\lambda_- - \Omega) - F^2)N_- & FGN_- \end{bmatrix}, \qquad (19)$$

where N_β's ($\beta = 0, \pm$) are the normalization factors given by $N_\beta = [\lambda_\beta^2 G^2 + (\lambda_\beta(\lambda_\beta - \Omega) - F^2)^2 + F^2 G^2]^{-1/2}$. Populations in the three dressed states will be the diagonal elements $\rho_{\beta\beta} = \langle \beta|\rho|\beta\rangle$, where $|\beta\rangle$'s are the three-orthonormal dressed eigenstates. Explicitly these dressed states are given by

$$|\beta\rangle = N_\beta\{FG|3\rangle - G\lambda_\beta|1\rangle + (\lambda_\beta(\lambda_\beta - \Omega) - F^2)|2\rangle\}. \qquad (20)$$

FIG. 9. Probe absorption spectra for $\Omega = 40$. The interference term (dot-dashed curve) is displaced by -0.05, units and the absorption term (dotted curve) is displaced by $+0.05$ units, along the Y axis for clarity. The net result is the solid curve. The other parameters are as in Fig. 5. Note the presence of Autler-Townes components around $\omega_{12} = \pm\Omega$, and Mollow-type features (see inset) around $\omega_{12} = \pm 2G, 0$.

ence of pronounced gain features around $|\Omega| = G$. We first ignore all the incoherent terms in Eq. (4). We can thus work with the state $|\phi\rangle$ of the system given by

$$|\phi\rangle = C_1(t)|1\rangle + C_2(t)|2\rangle + C_3(t)|3\rangle. \qquad (15)$$

Here $C_i(t)$ are the probability amplitudes of the states $|i\rangle$, $i = 1, 2$, and 3. For simplicity, we take $\Delta_2 = 0$ and treat the Rabi frequencies F and G as real. Substituting Eq. (15) into the Schrödinger equation along with the Hamiltonian (3) with only the pump field terms, we arrive at the matrix equation
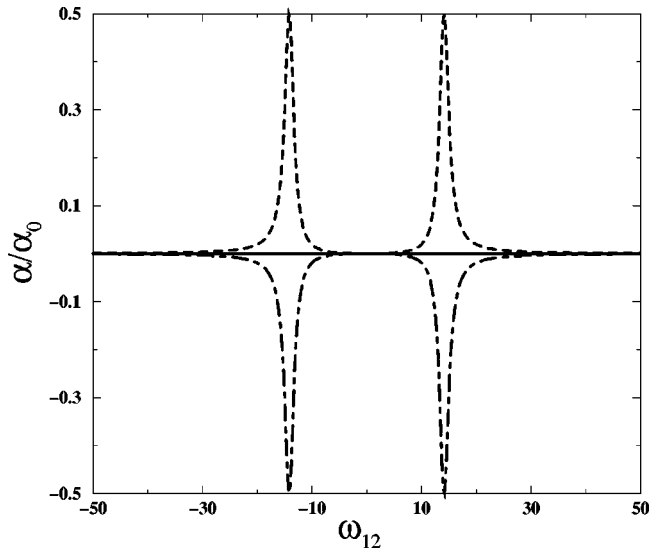

FIG. 10. Probe absorption spectra for $\Omega = 0$. The interference term (dot-dashed curve) and the absorption term (dashed curve) completely cancel each other, giving rise to transparency. The rest of the parameters are as in Fig. 5.
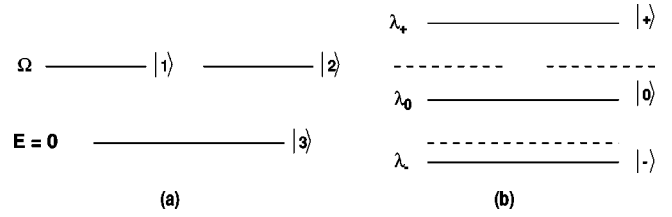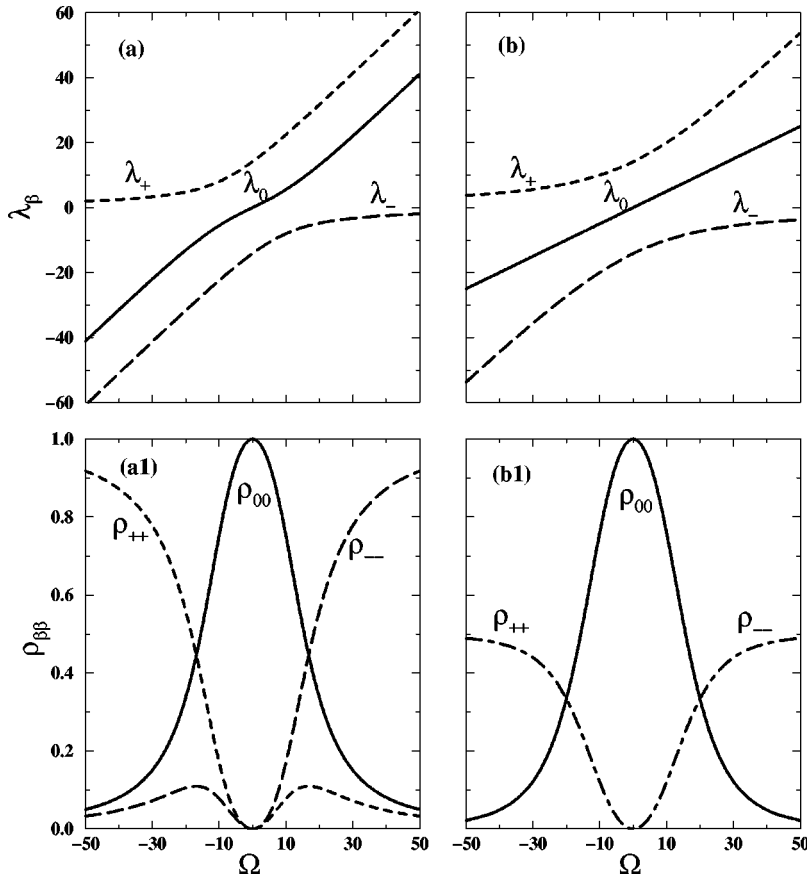
FIG. 12. Eigenvalues λ_β and the corresponding dressed-state populations $\rho_{\beta\beta}$ as a function of spacing Ω. Here $G=F=10$ and $\Delta_2=0$ for (a), while $\Delta_2=-\Omega/2$ for (b). Note that most of the population is in state $|0\rangle$ for $\Omega<2G$, giving rise to stimulated emissions, as shown in Fig. 13(b).

We evaluate the steady-state population of the three dressed states in the presence of dissipation terms by using Eqs. (4) (without the probe field terms) and (20). In Figs. 12(a1) and 12(b1), we plot the steady-state population in the three dressed states as a function of Ω. For $\Omega=0$ only the state $|0\rangle$ is occupied due to population trapping but for $\Omega\neq0$ there is still *population inversion* for $\Omega<2G$, thus giving rise to the possibility of stimulated emission from state $|0\rangle$. We also plot the population for the symmetric case when $\Delta_2=-\Omega/2$, and note that for this case, population in both the dressed states $|+\rangle$ and $|-\rangle$ are the same for all values of Ω. It should be noted that the weight factor for the state $|1\rangle$ is small in the state $|0\rangle$ compared to states $|\pm\rangle$ for the range of $\Omega\lesssim G$, because $\lambda_0<G$ for this range. Thus inversion in the dressed basis is a reflection of ground-state coherence and noninversion in the bare basis.

The various peaks in the absorption spectrum correspond to the transitions among the dressed states, and this can be seen from the quantized dressed-state description where the pump field is quantized. The classical nature of the laser modes is still preserved by taking mean number of photons $\langle n\rangle$ very large, and $\langle n\rangle\gg\Delta n\gg1$, where Δn is the fluctuation about the mean value $\langle n\rangle$. The Hamiltonian H_0 of the system without the interaction term is given by

$$H_0=\hbar(W_{13}A_{11}+\Omega A_{22})+\hbar\omega_2(a^\dagger a+1/2),\qquad(21)$$

where a and $a^\dagger$ are the annihilation and creation operators for the laser mode at frequency ω_2. The uncoupled eigen-

states for the above Hamiltonian with positive Ω are as shown in Fig. 13(a). The two manifolds $M(n-1)$ and $M(n)$ are shown and their centers have energy separation of $\hbar\omega_2$. The interaction with the field results in the mixing of various uncoupled eigenstates in a given manifold, and the eigenvalues for each manifold can be evaluated as done above. The pump field mixing the uncoupled eigenstates of two different manifolds can be neglected by invoking the RWA [19]. In a strict sense, all the atomic variables, the coupling strengths G and F and the eigenvalues will be different for different manifolds, but since we have assumed a laser mode with a large mean number of photons and a relatively narrow distribution, the difference between n and $n\pm1$ can be neglected. The dressed states in a given manifold, say $M(n-1)$, can be generalized from Eq. (20) by replacing states $|1\rangle$, $|2\rangle$, and $|3\rangle$ by the eigenstates of Eq. (21), i.e., $|1,n-1\rangle$, $|2,n\rangle$, and $|3,n\rangle$ respectively. The sequence of dressed states for two adjacent manifolds are shown in Fig. 13(b). Populations in the states $|\beta,n-1\rangle$ and $|\beta,n\rangle$ can be considered equal in the semiclassical limit, and a transition among these states correspond to the the pump frequency ω_2.

A. Case I: Emission from $|0,n\rangle$ states

As shown in Figs. 12(a1) and 12(b1), the population in state $|0\rangle$ is greater than that in $|\pm\rangle$ for $|\Omega|<2G$. This gives rise to the possibility of stimulated emission from states $|0,n\rangle$ to states $|\pm,n-1\rangle$ at probe frequencies $\omega_1=\omega_2+\lambda_0$
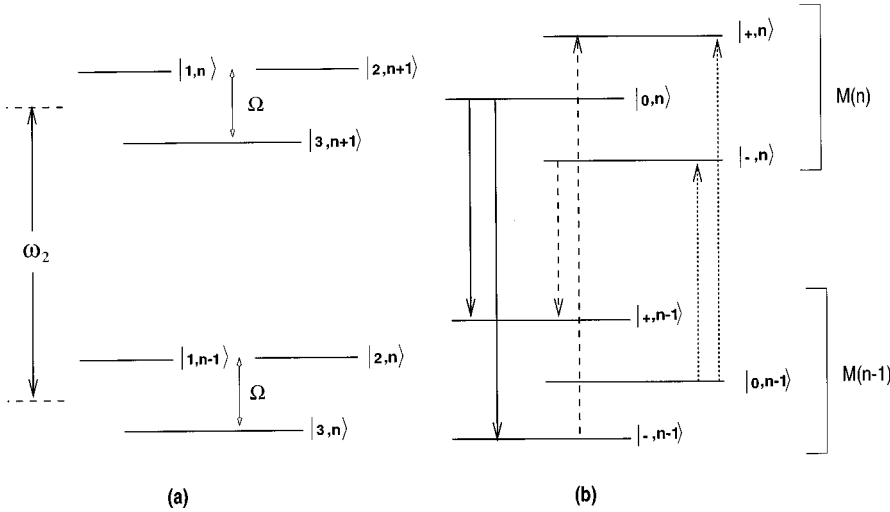
FIG. 13. Quantized dressed-state picture: (a) The uncoupled eigenstates of two adjacent manifolds $M(n)$ and $M(n-1)$ separated by pump photon energy $\omega_2(\hbar=1)$. (b) The corresponding dressed states when coupling is included. The arrows indicate various absorption and emission processes among the dressed states. As noted in Fig. 5, the interference minimizes the absorption from states $|0,n-1\rangle$, but enhances the stimulated emission from states $|0,n\rangle$.

$-\lambda_\pm$. For $\Omega=F=G=10$ and $\Delta_2=0$, $\lambda_+=22.46$, $\lambda_0=5.549$, and $\lambda_-=-8.02$. Thus there is a possibility of gain around $\omega_{12}=-16.9$ and 13.5 from the above analytical results, and this is in tune with the numerical result in Fig. 5. The small discrepancy in the numerical and analytical values arise because of the inclusion of dissipative terms in the numerical results. Both these gains can be understood phenomenologically in terms of three-photon gain. Two pump photons are absorbed along with the emission of a probe photon as shown in Fig. 14. We mention that the maximum value of gain at both these points is sensitive to the decay rates and decreases for unequal decay rates (numerical result not shown).

Apart from inversion it is the coupling of the dressed atom with the probe field that governs the enhancement of gain, and as we see for $|\Omega|\ll G$, though there is population inversion, the coupling strength reduces because the system is close to the CPT state. The coupling strength of the probe field will depend on the induced transition dipoles among the dressed states, given by

$$\vec{d}_{\alpha,\beta}=-N_\alpha N_\beta \lambda_\alpha G\{FG\vec{d}_{13}+(\lambda_\beta(\lambda_\beta-\Omega)-F^2)\vec{d}_{12}\}$$
$$\times e^{i(\omega_2+\lambda_\alpha-\lambda_\beta)t}. \qquad (22)$$

Here the indices α and β take values 0 and $\pm$. The above expression explains the existence of seven frequencies at
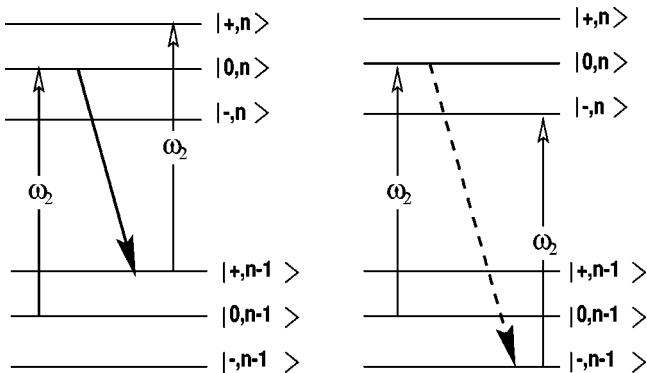

FIG. 14. Diagrammatic explanation of the two gain processes. The solid (dotted) arrow corresponds to three-photon gain at $\omega_2+\lambda_0-\lambda_+$ ($\omega_2+\lambda_0-\lambda_-$).

which the dipole moment of the dressed atom will oscillate. This explains seven different features at $\omega_{12}=\lambda_\alpha-\lambda_\beta$ in Fig. 5 (around $\omega_{12}\approx 0,\pm 13.5,\pm 16.9,\pm 30.4$). From the above expression it is evident that the gain components $\omega_2+\lambda_0-\lambda_\pm$ will have a coupling strength proportional to λ_0. As seen in Figs. 12(a) and 12(b) $\lambda_0\to 0$ for $|\Omega|\ll G$, and hence the coupling strength reduces in this region. The coupling is absent at $\Omega=0$. For $|\Omega|>G$, the population inversion reduces, and as an interplay between these two the optimum gain is observed only around $|\Omega|\approx G$. To clarify the existence of specific characteristic around $|\Omega|\approx G$ further, we plot one of the gain components $\omega_{12}=\lambda_0-\lambda_-$ as a function of Ω in Fig. 15, and compare it with the component at $\omega_{12}=\lambda_--\lambda_+$, the transition among extreme dressed states. Note that the gain features are prominent at $|\Omega|\approx G$ for $\omega_{12}=\lambda_0-\lambda_-$, and no such special features are seen for probe frequency at $\omega_{12}=\lambda_--\lambda_+$. This validates the point that stimulated emission from $|0,n\rangle$ is optimum only around $|\Omega|\approx G$.

B. Case II: Absorption from $|0,n-1\rangle$ states

In Fig. 5, note that the possibility of strong absorption at $\omega_{12}=-13.3$ and 16.6, is minimized by the interference term. This corresponds to the probe frequencies at $\omega_1=\omega_2+\lambda_\pm-\lambda_0$ [the dotted arrows in Fig. 13(b)], and we study in detail the reasons for this kind of *transparency*. In Fig. 16 we plot one of the components, $\omega_{12}=\lambda_+-\lambda_0$ as a function of Ω. As seen, the strong absorption is nullified by the interference term. The net absorption is zero at $\Omega=0$ due to formation of the CPT state, and continues to remain *minimum* for a range of $|\Omega|<2G$ due to state $|0\rangle$ being close to a CPT-like state. Physically this can be understood in terms of destructive interference leading to small dipole matrix elements for these transitions. This can be seen from expression (22), where we see that the frequency component at $\omega_2+\lambda_\pm-\lambda_0$ will have an induced dipole moment given by

$$-N_0 N_\pm \lambda_\pm G\{FG\vec{d}_{13}+(\lambda_0(\lambda_0-\Omega)-F^2)\vec{d}_{12}\}, \quad (23)$$

where $\lambda_0(\lambda_0-\Omega)-F^2<0$ for all values of Ω. This gives rise to opposite contributions from the dipoles oscillating along $|1\rangle\leftrightarrow|2\rangle$ and $|1\rangle\leftrightarrow|3\rangle$ transitions, and the amplitudes
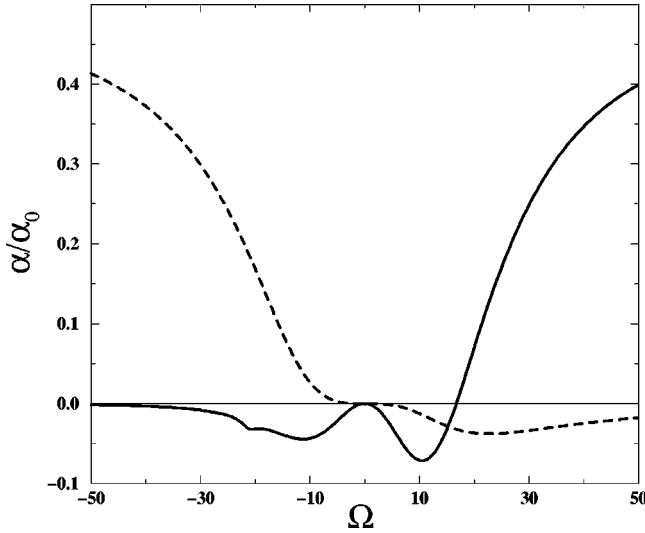
FIG. 15. Absorption coefficient at various values of probe frequencies as a function of Ω. The solid curve is for $\omega_{12}=\lambda_0-\lambda_-$, and the dotted curve for $\omega_{12}=\lambda_--\lambda_+$. Other parameters include $G=F=10$, $g=f=0.1$, and $\Delta_2=0$.

along these transitions hardly differ for $|\Omega| \lesssim G$. For frequency components at $\omega_2+\lambda_0-\lambda_\pm$ and $\omega_2+\lambda_\pm-\lambda_\mp$, the dipoles add up in phase because $\lambda_\pm(\lambda_\pm-\Omega)-F^2>0$ for all values of Ω. Thus the net coupling for these components are important for any $\Omega>0$. On the other hand, retaining the pump polarization and taking the probe polarization along $(\hat{\boldsymbol{\epsilon}}_2-\hat{\boldsymbol{\epsilon}}_3)/\sqrt{2}$ ($f=-g$), the coupling at $\omega_{12}=\lambda_\pm-\lambda_0$ will be the strongest compared to the other components.

C. Case III: Transition among $|\pm\rangle$ states

The extreme peaks in Fig. 5, the gain peak at $\omega_{12}=-30.4$, and the absorption peak at $\omega_{12}=30.4$ arise because of transition among extreme dressed states as shown in Fig. 13(b) with dashed lines. They correspond to the probe frequencies $\omega_1=\omega_2+\lambda_\pm-\lambda_\mp$. The gain at $\omega_1=\omega_2+\lambda_--\lambda_+$ is because of the small population inversion as seen in Fig. 12(a1) at $\Omega=10$. Also note from Figs. 12(a1) and 12(b1) that the population in these extreme states, unlike state $|0\rangle$, is very sensitive to the pump detuning. The gain will appear at $\omega_{12}=\lambda_--\lambda_+$ for $\Delta_2>-\Omega/2$, and at $\omega_{12}=\lambda_+-\lambda_-$ for $\Delta_2<-\Omega/2$ ($\Omega>0$). This is because unlike state $|0\rangle$ which has a major contribution from coherence due to cross talk, both $|\pm\rangle$ states have crucial contributions from optical coherences.

At $\Delta_2=-\Omega/2$ the plot for eigenvalues in Fig. 12(b) shows that $\lambda_+-\lambda_0=\lambda_0-\lambda_-$, because of the extreme eigenvalues placed symmetrically about λ_0 for all values of Ω. This explains the presence of very symmetric profiles about $\omega_{12}=0$ in Fig. 4. Also, as shown in Fig. 12(b1) the population in the extreme dressed states $|\pm\rangle$, are the same for all values of Ω. This gives rise to the dispersive kind of profiles as noted in Fig. 4 at $\omega_{12}=\lambda_\pm-\lambda_\mp$ due to the transition among dressed states of equal population. These dispersive profiles can be explained by taking into account the nonsecular terms in the dressed-state analysis [4,5]. The gain observed here is not because of any inversion, either in dressed states or in bare states, but due to coherence among dressed
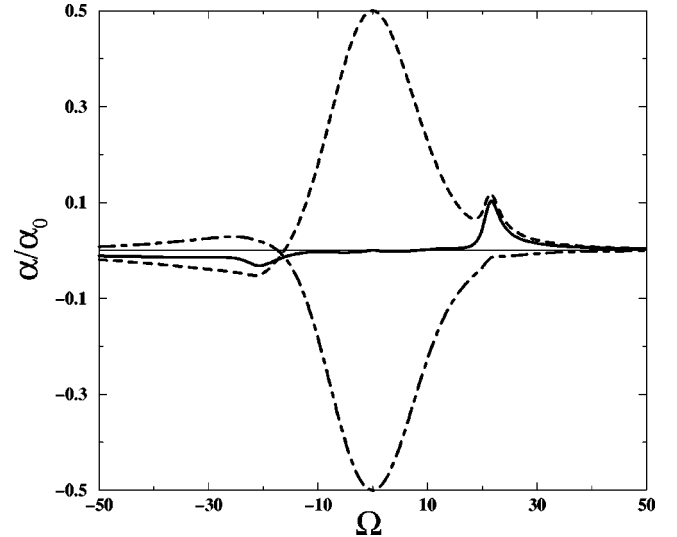

FIG. 16. Absorption coefficient for one of the transparency components at $\omega_{12}=\lambda_+-\lambda_0$ as a function of Ω. The interference term (dot-dashed curve) almost nullifies the absorption (dashed curve) for a range of $|\Omega|$ approximately up to G. There is a net transparency of around 99% in this range. The other parameters are as in Fig. 15.

states [17]. Further, at $\Omega=2G=-2\Delta_2$, the population in all the three dressed states are equal. This explains the presence of dispersive profiles even at $\omega_{12}=\pm(\lambda_0-\lambda_+)$ for this particular case.

V. CONCLUSIONS

In conclusion we have shown the possibility of both gain and weak transparency in a driven Λ system with closely spaced ground levels, due to cross talk among optical transitions. We have discussed the possibility of additional interference effects which enhance the gain at $|\Omega|\approx G,F$. Through a dressed-state description, we have shown that the origin of gain is due to population inversion among the dressed states. Further, the weak transparency at certain probe frequencies is due to weak coupling among dressed states. We have shown the existence of gain for probe-pump detuning both greater and less than zero for a given pump detuning, and have also noted the Mollow-type features appearing in a spectra of driven three-level systems.

Finally, we note that even incoherent vacuum field can generate coherence within near-degenerate levels with separation of the order of decay rates. Under suitable conditions interference effects can be seen [31,32], which recently have led to interesting applications like quenching of spontaneous emission [33], subnatural linewidths, gain without inversion [34], phase-dependent line shapes [35], etc. Effects of such terms will be analyzed in a future publication.

[1] B. R. Mollow, Phys. Rev. A **5**, 2217 (1972).

[2] F. Y. Wu, S. Ezekiel, M. Ducloy, and B. R. Mollow, Phys. Rev. Lett. **38**, 1077 (1977); A. Lezema, Y. Zhu, M. Kanskar, and T. W. Mossberg, Phys. Rev. A **41**, 1576 (1990); M. T. Gruneisen, K. R. MacDonald, and R. W. Boyd, J. Opt. Soc. Am. B **5**, 123 (1988); W. V. Davis, A. L. Gaeta, R. W. Boyd, and G. S. Agarwal, Phys. Rev. A **53**, 3625 (1996).

[3] S. Haroche and F. Hartmann, Phys. Rev. A **6**, 1280 (1972); G. S. Agarwal, Opt. Commun. **80**, 37 (1990); Phys. Rev. A **42**, 686 (1990); A. Karawajczyk, J. Zakrzewski, and W. Gawlik, *ibid.* **45**, 420 (1992); J. Zakrzewski, M. Lewenstein, and T. W. Mossberg, *ibid.* **44**, 7717 (1991).

[4] Dispersive gain profiles in a driven two-level system were explained by G. S. Agarwal, Phys. Rev. A **19**, 923 (1979).

[5] G. Grynberg and C. Cohen-Tannoudji, Opt. Commun. **96**, 150 (1993).

[6] R. W. Boyd, *Nonlinear Optics* (Academic, Boston, 1992), Chap. 5.

[7] S. E. Harris, Phys. Rev. Lett. **62**, 1033 (1989).

[8] O. Kocharovskaya and Ya. I. Khanin, Pis'ma Zh. Éksp. Teor. Fiz. **48**, 581 (1988) [JETP Lett. **48**, 630 (1988)].

[9] A. Imamoğlu, J. E. Field, and S. E. Harris, Phys. Rev. Lett. **66**, 1154 (1991).

[10] A. Imamoğlu and S. E. Harris, Opt. Lett. **14**, 1344 (1989); S. E. Harris and J. J. Macklin, Phys. Rev. A **40**, 4135 (1989); S. E. Harris, Phys. Today **50** (7), 36 (1997).

[11] M. O. Scully, S. Y. Zhu, and A. Gavrielides, Phys. Rev. Lett. **62**, 2813 (1989); L. M. Narducci, H. M. Doss, P. Ru, M. O. Scully, S. Y. Zhu, and C. Keitel, Opt. Commun. **81**, 379 (1991); M. O. Scully and M. Fleischhauer, Science **263**, 337 (1994).

[12] G. S. Agarwal, S. Ravi, and J. Cooper, Phys. Rev. A **41**, 4721 (1990); **41**, 4727 (1990); B. Prasad and G. S. Agarwal, Opt. Commun. **86**, 406 (1991); G. S. Agarwal, G. Vemuri, and T. W. Mossberg, Phys. Rev. A **48**, 4055 (1993).

[13] O. Kocharovskaya and P. Mandel, Phys. Rev. A **42**, 523 (1990); Opt. Commun. **77**, 215 (1990). For a review on the subject, see O. Kocharovskaya, Phys. Rep. **219**, 175 (1992).

[14] A. S. Zibrov, M. D. Lukin, D. E. Nikonov, L. Hollberg, M. O. Scully, V. L. Velichansky, and H. G. Robinson, Phys. Rev. Lett. **75**, 1499 (1995); G. G. Padmabandu, G. R. Welch, I. N. Shubin, E. S. Fry, D. E. Nikonov, M. D. Lukin, and M. O. Scully, *ibid.* **76**, 2053 (1996).

[15] A. Nottelmann, C. Peters, and W. Lange, Phys. Rev. Lett. **70**, 1783 (1993).

[16] W. E. van der Veer, R. J. J. van Diest, A. Dönszelmann, and H. B. van Linden van den Heuvell, Phys. Rev. Lett. **70**, 3243

(1993); F. B. de Jong, A. Mavromanolakis, R. Spreeuw, and H. B. van Linden van den Heuvell, Phys. Rev. A **57**, 4869 (1998).

[17] G. S. Agarwal, Phys. Rev. A **44**, R28 (1991).

[18] C. Cohen-Tannoudji and S. Reynaud, J. Phys. B **10**, 345 (1977); **10**, 2311 (1977); L. M. Narducci, M. O. Scully, G.-L. Oppo, P. Ru, and J. R. Tredicce, Phys. Rev. A **42**, 1630 (1990); G. S. Agarwal and S. S. Jha, J. Phys. B **12**, 2655 (1979).

[19] For a detailed discussion, see C. Cohen-Tannoudji, J. Dupont-Roc, and G. Grynberg, *Atom-Photon Interactions: Basic Processes and Applications* (John Wiley & Sons, New York, 1992), Chap. VI.

[20] C. Cohen-Tannoudji and S. Reynaud, J. Phys. B **10**, 365 (1977).

[21] D. F. Walls and P. Zoller, Opt. Commun. **34**, 260 (1990); G. P. Agrawal, Phys. Rev. A **24**, 1399 (1981).

[22] H. M. Concannon, W. J. Brown, J. R. Gardner, and D. J. Gauthier, Phys. Rev. A **56**, 1519 (1997).

[23] H. Xia, S. J. Sharpe, A. J. Merriam, and S. E. Harris, Phys. Rev. A **56**, R3362 (1997).

[24] J. Javanainen, Europhys. Lett. **17**, 407 (1992).

[25] S. H. Autler and C. H. Townes, Phys. Rev. **100**, 703 (1955).

[26] D. Grandclement, G. Grynberg, and M. Pinard, Phys. Rev. Lett. **59**, 40 (1987); G. Grynberg and P. R. Berman, Phys. Rev. A **39**, 4016 (1989).

[27] W. J. Brown, J. R. Gardner, D. J. Gauthier, and R. Vilaseca, Phys. Rev. A **56**, 3255 (1997).

[28] M. O. Scully, Phys. Rev. Lett. **67**, 1855 (1991).

[29] The effect of a relative angle between pump and probe field polarizations on probe absorption was also noted in Ref. [20].

[30] For a review article on coherent population trapping, see E. Arimondo, in *Progress in Optics*, edited by E. Wolf (North-Holland, Amsterdam, 1996), Vol. XXXV, p. 257, and references therein.

[31] G. S. Agarwal, *Quantum Statistical Theories of Spontaneous Emission and Their Relation to Other Approaches* (Springer-Verlag, Berlin, 1974), p. 95.

[32] D. A. Cardimona, M. G. Raymer, and C. R. Stroud, J. Phys. B **15**, 55 (1982).

[33] M. O. Scully, S. Y. Zhu, and A. Gavrielides, Phys. Rev. Lett. **62**, 2813 (1989); H. R. Xia, C. Y. Ye, and S. Y. Zhu, *ibid.* **77**, 1032 (1996); H. Lee, P. Polynkin, M. O. Scully, and S. Y. Zhu, Phys. Rev. A **55**, 4454 (1997); G. S. Agarwal, *ibid.* **55**, 2457 (1997).

[34] P. Zhou and S. Swain, Phys. Rev. Lett. **78**, 832 (1997); Phys. Rev. A **56**, 3011 (1997).

[35] S. Menon and G. S. Agarwal, Phys. Rev. A **57**, 4014 (1998).